Monitoring satellite radiance biases using NWP models

R.W. Saunders, T. Blackmore, B. Candy, P.N. Francis and T.J. Hewison

Abstract— **Radiances measured by satellite radiometers are often subject to biases due to limitations in their radiometric calibration. In support of the Global Space-Based Intercalibration System (GSICS) project, to improve the quality of calibrated radiances from atmospheric sounders and imaging radiometers, an activity is underway to compare routinely measured radiances with those simulated from operational global numerical weather prediction (NWP) fields. This paper describes the results obtained from the first three years of these comparisons. Data from the HIRS, SEVIRI, AATSR, AMSU and MHS radiometers together with AIRS, a spectrometer, and IASI, an interferometer, were included in the analysis. Changes in mean biases and their standard deviations were used to investigate the temporal stability of the bias and radiometric noise of the instruments. A double difference technique can be employed to remove the effect of changes or deficiencies in the NWP model which can contribute to the biases. The variation of the biases with other variables was also investigated such as scene temperature, scan angle, location and time of day. Many of the instruments were shown to be stable in time, with a few exceptions, but measurements from the same instrument on different platforms are often biased with respect to each other. The limitations of the polar simultaneous nadir overpasses often used to monitor biases between polar orbiting sensors are shown with these results due to the apparent strong dependence of some radiance biases with scene temperature.**

Index Terms— **Calibration, NWP models, Remote Sensing, Satellites**

I. INTRODUCTION

The operational assimilation of satellite radiances in numerical weather prediction (NWP) models provides a continuous record of the difference between the measured radiances and the equivalent simulated values computed from model fields coupled with a radiative transfer (RT) model. These differences can be due to biases in the instrument calibration or anomalies in the instrument operation which is information of value to space agencies, if available in near real time. They can also be due to the NWP models which can have consistent biases in their representation of the atmosphere/surface (e.g. water vapour concentration, surface skin temperature), but these biases do not change rapidly in time except when linked to the diurnal cycle. Also, but to a lesser extent, the RT model used to simulate the radiances may introduce a bias especially for broad spectral channels where the fast RT model assumptions start to break down. These NWP and RT model biases should, in general, remain the same for different instruments with channels at similar wavelengths and so should cancel out when the biases between two instruments inferred from the same NWP system are differenced. It is only when interpreting the absolute value of the observed–simulated radiance biases that the model biases need to be considered. For temperature sounding channels with weighting functions which peak in the troposphere the simulations should be accurate to better than 1K for current state-of-the-art NWP and RT models, but for water vapour channels the 3 dimensional representation of water vapour in NWP models is known to have biases in some regions [1]. Before assimilation in a variational analysis which assumes unbiased Gaussian statistics these biases have to be removed using a correction scheme [2], [3]. To calculate the effects of other gases (e.g. ozone) only climatological mean profiles are used in most NWP models and so large biases are to be expected in the model simulations of channels which are affected by these trace gases.

One of the objectives of the Global Space-based Intercalibration System (GSICS) [4] is to understand the nature of the biases seen in radiances measured by satellite instruments. These include radiometers, spectrometers and interferometers with the two latter sensors providing much higher spectral resolution. These biases can be due to uncertainties in the calibration of the sensor and can vary with time on orbital, daily and seasonal timescales. The current approach of comparing the filter radiometers (e.g. HIRS, SEVIRI) with high spectral resolution spectrometers or interferometers (e.g. AIRS, IASI) for simultaneous near nadir overpasses (SNOs) has been used with some success [5]-[7] but the area and time window available for these coincidences is very limited. Recent studies have shown [8] that the limited high latitude SNOs from polar orbiting satellites do not provide an adequate sampling of the instrument biases for a full range of atmospheric conditions. SNOs do however allow comparisons over a much wider range of scene temperatures

Manuscript received February 9, 2012. This work was funded by EUMETSAT under several contracts.

R.W. Saunders, B. Candy, P.N. Francis and T. Blackmore are with the Met Office, Fitzroy Rd., Exeter, U.K. EX1 3PB. T. Hewison is with EUMETSAT, Eumetsat-Allee 1, 64295 Darmstadt, Germany

Corresponding author R.W. Saunders (phone: +44-1392-886295; e-mail: roger.saunders@metoffice.gov.uk).

than is possible with clear sky only comparisons. Other studies using vicarious calibration from fixed test sites have also been made [9] but they suffer from limited sampling of the scene temperatures.

Any non-linearities in the radiometric calibration or similar effects result in inter-satellite biases which can vary with scene temperature and hence latitude. By comparing not only the radiances themselves but their biases, determined by comparisons with radiances simulated from a global NWP model, more can be learnt about their global nature [10], [11]. In addition the biases computed inherently take into account differences due to spectral responses varying between common channels as the RT model calculation takes account of this. For climate applications it has been stated [12] that an absolute calibration accuracy must be less than 0.1K in order to be able to unambiguously determine trends. It is crucial for climate monitoring and also beneficial for NWP that we understand the characteristics of these radiance biases and the GSICS program [13] is focused on providing some new information in this area. Before Fundamental (level 1) and Thematic (level 2) Climate Data Records are produced from the radiances any biases must be characterized and removed.

This paper describes some results over a period of 3 years from November 2008 to November 2011 when the biases of a number of instruments compared with simulations from the Met Office global NWP model were analysed. The fast radiative transfer model coupled with the Met Office Unified global NWP model is described in section 2, the satellite data and processing is outlined in section 3, the methodology to compute the biases is given in section 4 and an analysis of the results in section 5 followed by a summary.

II. NWP AND RADIATIVE TRANSFER MODEL DESCRIPTION

The NWP suite used for computing the simulated satellite radiances is the global version of the Unified Model (UM) at the Met Office used operationally for its weather forecasting and climate modeling applications [14], [15]. A diverse range of observations from in-situ and satellite systems are assimilated in the 4D variational analysis [16] used to define the initial atmospheric state for the forecast runs.

The background profile values, from a 6 hr forecast off the most recent analysis, on the model grid are interpolated to the observation location and time. The model variables required for the calculation are profiles of temperature, water vapour concentration, ozone concentration, surface temperature (2m and skin), wind speed (over ocean only) and surface pressure. Ozone, which affects some channels, is only represented by a climatological distribution [17] which is based on a reference profile (to give the vertical distribution) in the UM and then scaled by the 70hPa temperature to give a total column amount. This scaling is based on a regression of 6 years of ozone retrievals with 70hPa temperatures for each month. There is no active representation of other trace gases, which are assumed to have a fixed concentration in the RT calculations, or aerosols in the data assimilation at present. The assumed CO_2 concentration was for the year 2005. The lack of accurate ozone profile information in reality affects only one set of channels used in this study around 1039cm^{-1} as shown in the sensitivity analysis to ozone in the right hand column of Table 1. All other effects from trace gases should be well below 0.1K for the channels selected for this study. The only other factor will be the extinction caused by high aerosol concentrations although for major outbreaks all the cloud detection schemes will identify these radiances as cloud contaminated.

The OSTIA sea surface temperature analysis [18] is used to define the skin temperature over the ocean but no allowance is made for the cooling of the skin at night (~0.15K) or any warming due to diurnal thermoclines in the day. The model forecast profiles of temperature, humidity, ozone and surface parameters at the observation locations are input to RTTOV-7, the fast radiative transfer model [19] used to compute the required radiances for the channels of interest for a specific instrument. It is important that the same version of the radiative transfer model is used throughout to ensure a consistent calculation of the simulated radiances. Broad band channels (e.g. SEVIRI 3.9μm channel) can have biases introduced by the RT model due to the fast model assumptions breaking down. Over the ocean the infrared surface emissivity was computed from the ISEM model [20] which is part of RTTOV. Over the land an emissivity of 0.98 was used, irrespective of wavelength and location and over sea-ice a value of 0.99 was chosen. For the microwave instruments FASTEM-2 [21] was used to compute the emissivities over ocean and a value of 0.95 is assumed over land and first year ice and 0.84 for multi-year ice.

Uncertainties in the surface skin temperature (and emissivity) from the NWP model can introduce significant biases in the radiative transfer simulations but these will affect different instruments in the same way. In most cases for the surface sensing channels only biases over the cloud-free ocean are presented here as they are expected to be small (<0.1K) although biases over land can also be analyzed with the dataset collected.

The operational UM and data assimilation systems are periodically updated to introduce improvements. There were several changes made which could affect the radiances simulated from the model fields which are listed in Table 2. The impact of some of these changes will be seen in the analysis of the biases presented below. Although the absolute bias of some channels may be affected, all instruments with similar channels will be affected in the same way.

The assimilation of satellite radiances in a variational data assimilation system requires that the radiances are unbiased with respect to the model background. As a result the Met Office has developed a bias correction scheme based on the Harris and Kelly [2] methodology as described in [22], [23]. This is applied to all the radiance sensors currently being assimilated at the Met Office which include ATOVS, AIRS, IASI and SEVIRI. A suite of programs is run every model cycle (6 hours) to generate Observed–Background clear sky radiances (hereafter referred to as O-B) where the background, B, are radiances generated from a 6 hour forecast set of profiles from the previous analysis of the UM and O are the observed top of atmosphere radiances. Both O and B are converted into equivalent black body brightness temperature (hereafter referred to as brightness temperature) to ease their interpretation. Both uncorrected (for this study) and bias corrected (for assimilation) radiances are computed. The routine monitoring of radiances at the Met Office is presented on the NWP Satellite Application Facility web site[1] for a variety of satellite sensors.

III. Satellite Data Processing

Table 3 lists the instruments for which data were processed as part of this study. There are a few gaps in data due to operational problems with various instruments as noted and data collection for AATSR only commenced in September 2010. When Meteosat-9 data dropped out, Meteosat-8 data were substituted but the statistics were kept separate. Data from the microwave sensors were included as indicated in Table 3 but the routine monitoring for these sensors did not begin until August 2010. The sources of the data are also indicated in Table 3. Note that only the global datasets are included here, not the EUMETSAT rebroadcast or EARS data or locally received HRPT/HRIT data.

The channels which were included in the analysis for each of the infrared instruments are defined in Table 1 using the normal channel numbering convention for each instrument. The criterion for the selection of the IASI and AIRS channels was proximity to the HIRS and/or SEVIRI channels so that comparisons could be made between different instruments at similar wavelengths. Note that the AIRS or IASI radiances were not integrated over the HIRS channels spectral responses as the aim was to monitor the stability of the individual channel radiances.

The Meteosat SEVIRI dataset received on EUMETCAST includes all pixels and covers the full Earth disk seen by SEVIRI and contains calibrated radiances. Data during the eclipse periods are removed for slots ±1hr from midnight to avoid spurious biases from solar radiation intrusions into the radiometer. The dataset used for this study samples every 4th pixel and scan line, and a cloud detection scheme [24] is used at the Met Office for generating its clear sky and cloud products for NWP assimilation and nowcasting applications. Very occasionally gaps for a single slot in the SEVIRI radiance time series occur thought to be due to missing data segments.

The global polar orbiter data are received from NOAA/NESDIS and EUMETSAT as calibrated radiances and processed to a common field of view by the AAPP (ATOVS and AVHRR Pre-Processing Package) software provided by the NWP SAF for ATOVS and IASI [25]. The radiances (which have had a correction applied to remove the mean bias) are then passed through a 1D-Var pre-processor which allows a quality control check and a cloud cost to be computed based on a Bayesian cloud test [26] using only infrared channels for IASI and HIRS and a separate cloud test for AIRS [27]. The IASI channel subset is taken from the clearest of the 4 fields of view within the corresponding Metop-A AMSU-A field of view. The AIRS radiances are taken from the warmest field of view within an Aqua AMSU-A field of view. One source of possible bias is due to undetected cloud in the measured radiances and so for this study it is important to have very strict cloud detection criteria. As a check on the removal of cloudy pixels, histograms of the clear sky radiances were examined and were shown to be Gaussian in shape and did not exhibit a ‘cold tail’.

AATSR radiances are averaged values over 10 arc minute cells and only cloud-free data are provided in the datasets (nominally for sea surface temperature, SST, retrievals) using the method described in [28]. For each averaged radiance the number of cloud-free pixels in the grid box is also provided. Although the data are cloud cleared, experience has shown from the SST retrievals that a more rigorous cloud check is desirable. Additional cloudy flags for the cell are set if the number of clear pixels is less than 15% of the maximum possible number of pixels in the 10 arc-minute cell (nadir view) or less than 10% (forward view). This is consistent with the operational AATSR SST processing at the Met Office [29]. The maximum number of pixels in a cell is latitude-dependent. An additional AATSR cloud detection O-B test is included as some pixels over uniform low stratus cloud were remaining undetected. If the **O – B** value is less than -4K for the 11 and 12 micron channels then the data are flagged as cloudy but this only rejected a few more pixels in persistently cloudy areas. Both the nadir and forward view AATSR radiances are included in the monitoring and kept separate to allow statistics for both sets to remain independent. Note ENVISAT overpass time is in a morning orbit similar to that of Metop-A. In late October 2010 there was a change to the ENVISAT orbit which resulted in a gap in the data stream of about a week but the quality of the data after the manoeuvre appeared to be maintained. There is a climate-quality AATSR dataset generated under the ARC project [30] but this is only

[1] http://research.metoffice.gov.uk/research/interproj/nwpsaf/monitoring.html

available for historical data at present and so could not be used for this analysis.

The AMSU and MHS pre-processing, in common with HIRS, uses the AAPP software [25]. The calibrated AMSU/MHS radiances are all mapped to the HIRS fields of view and tests are applied to identify those affected by hydrometeors and complex surfaces in the microwave. A scattering index and minimising a cost function are used to identify microwave 'clear-sky' fields of view.

Only radiances which have passed the quality control checks and converged in 1D-Var are used for computing the **O – B** bias. For this study variables such as incidence angle, latitude and longitude are all stored with each observation in the bias datasets to enable the required analysis. These datasets have been generated from 19 November 2008 (just before the Meteosat-9 SEVIRI decontamination was performed) up to 1 December 2011 for all sensors except AMSU/MHS and the AATSR instruments which started from August/September 2010. The processing is now continuing as part of the EUMETSAT NWP SAF activities. AATSR data collection ceased on the 8 April 2012 when all contact with the Envisat satellite was lost.

IV. Methodology for Analysis

The overall technique of using NWP models to monitor radiance biases is outlined in recent papers [10], [31] who have applied this technique to AVHRR (Advanced Very High Resolution Radiometer) and TES (Tropospheric Emission Spectrometer) radiances respectively. In summary the mean bias referred to here as **O – B** can be given for a channel n averaged over the region of interest for instrument j as:

$$\delta B_j(n) = \frac{1}{k}\sum_{i=1}^{i=k}[y_n - H_n^j(x_i)]$$

where the number of quality controlled clear sky radiances y_n in the region is k, $H_n(x_i)$ is the radiative transfer model using the background model state x_i for observation i. For another instrument m with a similar channel n' we have for an observation i':

$$\delta B_m(n') = \frac{1}{k}\sum_{i'=1}^{i'=k}[y_{n'} - H_{n'}^m(x_{i'})]$$

If the centre wavelengths of the channels are similar and the atmospheric absorption and surface emissivity are not changing rapidly with wavelength we can assume the bias from the model simulations will be the same. Assuming they are the same we can then do a ***double difference*** between different sensors:

$$D_{j-m} = \delta B_j(n) - \delta B_m(n')$$

where D_{j-m} should be independent of any biases from the NWP and radiative transfer model and relate to the instrument biases either through errors in the calibration of the instruments or the spectral response of the channel.

In addition to the bias, the variance of the **O** - **B** differences over the region of interest can also be computed. If the model background errors are stable and small enough (e.g. <0.5K rms for temperature profiles) this can, in some cases, be a measure of the instrument radiometric noise and any other varying effects (e.g. modulation around an orbit). To carry out a statistical analysis of the radiance biases they are averaged over various regions defined as global, tropical (± 30˚ latitude), N. Hemisphere (+30˚ to +60˚ latitude) and S. Hemisphere (-30˚ to -60˚ latitude) and the SEVIRI area defined by the area of the Earth's disk viewed by SEVIRI up to incidence angles of 68˚. Table 4 lists the sampling bins which the biases are stored for subsequent statistical analysis of their dependencies on location, incidence angle, scene temperature, time of day, etc.

V. Analysis of Radiance Biases

Data for the period Nov 2008 to Nov 2011 have been analysed to show the variation in the clear sky **O – B** biases globally over the ocean for different sensors as a function of a number of variables. The results are summarised here.

A. Annual Global Means

The number of observations recorded for each sensor is documented in Table 5. Currently over 10^8 observations for each sensor are included in the global datasets and so the statistical uncertainty is negligible even after binning the data. Note that for those shortwave channels affected by solar radiation during the day only the night-time data are used in the statistics here as no fast forward model for the reflected solar component was available.

The overall **O-B** statistics for 2010 for each of the infrared radiometers are plotted in Figure 1 for channels closest to the HIRS channel as defined in Table 1. The global mean biases over the sea for each of the HIRS and corresponding SEVIRI and AATSR channels are plotted in Figure 1 and also tabulated in Tables 6 to 8. The main points to note are:

- With the exception of the ozone channels (denoted channel 9), the SEVIRI 13.4µm CO_2 (HIRS channel 7) and 3.9µm window channels (HIRS channel 19) all the biases with respect to the NWP model are less than ±1.5K.
- The large bias for the SEVIRI 13.4µm CO_2 channel (HIRS channel 7) is explained below. For the 3.9µm channel (HIRS channel 19) this is partly due to a bias from the fast RT model as the channel has a very broad

spectral response compared to the corresponding HIRS channel.
- Most of the HIRS channel biases are similar for each instrument with the exception of channels 13 and 16 on NOAA-17 and channel 1 on NOAA-19.
- Not shown but the biases for 2009 were very similar to those in 2010 except for the biases of the NOAA-17 HIRS longwave stratospheric sounding channels which have progressively increased (become more negative) with time.
- The two AATSR channels plotted show lower biases and standard deviations (Figure 2) than the corresponding HIRS/SEVIRI channels demonstrating the value in using this instrument as the reference and also suggesting the HIRS and SEVIRI biases may be instrument rather than model related or their O-B statistics are both more affected by residual cloud.
- The magnitude of the biases between sensors is an order of magnitude larger than the specified requirement of <0.1K for climate applications

The standard deviation of the global O-B differences are plotted in Figure 2 and here with the exception of NOAA-17 HIRS channel 1 all instruments are in agreement, with the model error dominating for the ozone (HIRS channel 9) and water vapour channels (HIRS 11 and 12). The noise on the HIRS channel 1 on NOAA-17 in 2010 has increased from 2009 by 50%. This shows the NOAA-17 HIRS detector or filter response is changing with time making it difficult to use the longwave CO_2 channels. However the other channels were still performing well after 10 years in orbit.

AIRS and IASI radiance biases for clear sky over the ocean for the channels in Table 1 are plotted in Figure 3 (bias) and Figure 4 (standard deviation) with biases for 2009 and 2010 plotted separately. As for HIRS with a few exceptions mentioned below all the biases are ±1K or less and the biases for AIRS and IASI are similar at the same frequencies suggesting they are probably due to the NWP or RT model. The AIRS and IASI channels at 668cm^{-1} have a larger bias and standard deviation due to their peaking high in the stratosphere where the model error in temperature is larger. The effect of an increase in the number of NWP model levels (50 to 70 levels) are also shown with a significant reduction in the bias and standard deviation for 2010. As the channels for the two advanced IR sounders are not identical the biases cannot be expected to be exactly the same especially for the high-peaking channels in rapidly changing spectroscopy. The standard deviation of the IASI channels in the long wave CO_2 band <900cm^{-1} is slightly less than the corresponding AIRS channels except at 668cm^{-1} where the model error dominates. In contrast the standard deviation of the IASI channels in the short wave CO_2 band >2000cm^{-1} is significantly higher than the corresponding AIRS channels. In some cases this is due to high-peaking channels being sensitive to the larger NWP model temperature biases and in other cases it is due to the higher radiometric noise of IASI compared to AIRS at these wavelengths.

For the ozone channels the bias and standard deviation are similar to that of the HIRS/SEVIRI ozone channels due to the unrepresentative ozone profile assumed in the RT model as also observed with the radiometer biases in Figure 2.

B. Time Series

The stability of the radiometer measurements over time is important to determine for NWP, reanalysis and climate monitoring applications. Time series plots of global mean O-B values are one way to determine the stability particularly if the double difference is employed to remove the effect of model changes.

An example of the time series of global mean O-B values for the SEVIRI 13.4µm CO_2 channels of all the infrared sensors is shown in Figure 5 for clear sky ocean radiances averaged over the SEVIRI full disk area. The start of this plot is just before the SEVIRI radiometer was heated up to remove accumulated ice on the detectors in late November 2008. The sudden change in the O-B bias of +0.7K after the decontamination is evident followed by the drift in the bias during the subsequent two and a half years from -1K to -2.9K probably due to the build up of water ice on the optics/detector [32]. The increase in bias is not uniform and during certain periods the change in bias is faster than others. This makes its use for climate monitoring, data assimilation and cloud detection problematic unless an adaptive bias correction is used for this channel. The spectral response of the channel will also change with the ice build up which will make the channel sensitive to a different level in the atmosphere also potentially contributing to the bias and a height error in the peak of the Jacobian. The bias of the other HIRS 13.3µm channels and corresponding AIRS and IASI channels also plotted in Figure 5 show a gradual change in the bias of about -0.3K over 3 years. This is due to the assumption of a fixed CO_2 mixing ratio in the radiative transfer model whereas in reality the CO_2 concentration has increased by 1.5% over the period. Simulations show that, for a +6ppmv increase in CO_2 (the increase from 2009-2011), the HIRS channel 7 brightness temperature decreases by 0.1K, less than observed, whereas the SEVIRI channel 11 decreases by only 0.08K. It is worth noting that all the HIRS instruments have similar biases but IASI has a more positive bias which is closer to zero and this may be due to the fact it is more sensitive to the lower atmospheric layers than the other instruments.

Figure 6 shows a plot for the SEVIRI 6.2µm water vapour channel and the corresponding HIRS channel (12). Here the biases of both channels vary significantly over the period due to changing biases in the NWP model upper tropospheric water vapour concentration but both instruments follow each other. The double difference in the lower panel is stable between SEVIRI and HIRS. The sudden change in bias and standard deviation of all the instruments, particularly for

SEVIRI and HIRS is where the bias is reduced by 0.3K due to the model change in the radiosonde water vapour bias correction in November 2009. Of more interest is the standard deviation of the difference where a significant decrease is seen by the HIRS and SEVIRI channels over the 3 years suggesting a gradual improvement in the model's representation of upper tropospheric water vapour.

When Meteosat-9 experienced an anomaly there were a few short periods when its radiances were replaced by Meteosat-8. The corresponding Meteosat-8 SEVIRI O-B biases for channel 11 (13.4μm) had a mean difference relative to Meteosat-9 of +1.2K in the bias with Meteosat-9 having the larger negative bias (not shown). This illustrates the problems when trying to derive climate data records from these instruments with the same channels but significantly different inherent biases.

The biases for the 11μm window channels of each instrument are plotted in Figure 7 for clear sky over ocean in the SEVIRI full disk area. As for other channels the HIRS biases are all very similar and quite negative (~-0.8K). A small negative bias is to be expected (~-0.15K) due to the cooling of the skin of the ocean at night. SEVIRI and IASI have very similar biases (~-0.3K) and AIRS is much closer to zero. AATSR, only available for the last 1 year and 3 months, has a mean cool bias of -0.2K which is close to that expected. What is also evident in Figure 7 is a sudden change in the bias in March 2010 for all instruments which corresponds to the introduction of the AMSU-A and SSMIS window channels into the assimilation system which affected the low level water vapour concentrations in the model and hence the simulated radiances for these channels. The IASI channel was less affected by this as it was a "cleaner" window channel with lower sensitivity to water vapour compared to the other instruments.

Radiance biases for the AMSU/MHS microwave channels were also collected but only for just over a year. Microwave sensors are in general very stable with time but can be subject to radio frequency interference (RFI) and sudden degradations in the receivers. Figure 8 shows the mean bias and standard deviation of the difference for the high-peaking water vapour MHS channel (3) on Metop-A and NOAA-19. The biases are different for each sensor but the double difference shows they are stable with respect to each other. It is the same for the other lower-peaking water vapour channels (not shown). The change in bias and standard deviation over time are similar to those seen in Figure 6 for the infrared water vapour channel which senses the same part of the atmosphere. Note these two figures are for different areas (i.e. SEVIRI disk vs global).

C. *Geographical Variations in Bias*

For the polar orbiting instruments biases changing around an orbit are possible due to sudden changes in the instrument temperature (e.g. as the satellite crosses the terminator) or occasional intrusion of solar radiation. The biases seen with the SSMIS radiometer provide a good example of biases which vary consistently around an orbit [33].

The geographical variation of the biases of different instruments is illustrated for the 11μm window channels in Figure 9, which shows maps of SEVIRI, AATSR and IASI biases for clear sky radiances over the ocean. All the biases are negative but whereas IASI biases are closer to zero at ~-0.2 to -0.4K SEVIRI has a bias of typically -0.4K to -0.6K. AATSR has a lower bias in the Tropics and S. Hemisphere (<0.3K) than IASI but a similar bias to IASI for the extratropical N. Hemisphere band. In contrast the 6.2μm water vapour channel biases (not shown) are similar for SEVIRI, HIRS and IASI suggesting the bias in this case is arising from the NWP model not the instruments in this case.

D. *Scene Dependent Bias*

Infrared and microwave radiometers are assumed to have a linear response with incident radiation but for a variety of reasons (i.e. detector response, use of space view as calibration reference) small non-linearities are often present. These can be measured during instrument characterisation before launch but if not adequately taken into account then a bias which varies with scene temperature [34] can be seen. Another possible cause, not due to the instruments, is the influence of undetected cloud for colder scene temperatures.

The observed changes in bias of the 11μm window channels for several instruments as a function of scene temperature between 260K and 300K are given in Figure 10. A limitation of our method using only clear sky radiances is that the colder scene temperatures for high cold cloud tops are not sampled. For HIRS the top two panels for Metop-A and NOAA-17 show a reduction in the negative bias with increasing scene temperature. SEVIRI shows a similar trend with zero bias for a scene temperature of 305K. AIRS and IASI also show similar trends of an increasing positive bias with scene temperature which is consistent with other results [34]. It is interesting to note that AATSR shows no trend for either the nadir or the forward views and this maybe because it has 2 blackbodies one at 305K and one at 256K. The other sensors only have one blackbody typically at 280K and use space as the cold target. Another possible explanation is that AATSR has better cloud detection at low scene temperatures. This was investigated by comparing the AATSR night-time only data (where only IR channels are used for the cloud detection) with the daytime data (where visible channels are also used). The shape of the bias curve was unchanged from day to night although the overall bias was slightly less during the day for all scene temperatures. The change in bias with scene temperature for other channels (e.g. 13.4μm and 6.2μm) exhibits a similar increase with scene temperature to that seen at 11μm.

Another conclusion to be drawn here is that the traditional polar SNOs commonly used to compare biases from different radiometers will only sample a narrow range of cold scene

temperature and hence will not measure a bias representative of the global mean. It has also been demonstrated through SNOs of polar orbiters at all latitudes which become possible for short periods due to orbit drift [8].

E. Satellite Zenith Angle Dependence

It is well known that cross-track sounders have scan dependent biases due to the changing reflective properties of the scan mirrors with incidence angle. For microwave instruments the side lobes in the antenna pattern also provide a contribution to the radiance which can be from parts of the spacecraft around the instrument. The first component of the bias correction schemes employed by NWP centres [2] attempts to remove this scan bias before applying a second step to remove the remaining airmass dependent bias. For the biases computed here it should be borne in mind that a constant sea surface emissivity is assumed for all viewing angles in the infrared simulations. For the microwave channels the FASTEM-2 model does allow for viewing angle changes in emissivity.

Plots of the bias as a function of viewing incidence angle at the surface appear to be different for each instrument even between the cross track sounders. For the 11μm channels Figure 11 shows the cross-track variation in the biases. The HIRS channel 8 biases for three different satellites show a very similar behaviour with symmetrically increasing biases away from the nadir view with magnitudes of 0.3K from nadir to the edge of the scan. IASI also exhibits a similar behaviour but with half the magnitude and in the opposite sense (lower biases at the swath edge) suggesting that the properties of the HIRS scan mirrors introduce a scan dependent calibration error. Although the SEVIRI imaging radiometer has a different viewing configuration the dependence on incidence angle is the same as for HIRS. AATSR with an offset conical scan of the surface shows no consistent changes in bias over its limited scan angle range for the nadir view but the forward view bias is 0.08K larger. The fact that the change in HIRS and IASI scan biases are of opposite sign suggests the impact of the fixed model emissivity on the results is negligible. AIRS biases (not shown) are slightly larger than for IASI but are much smaller than HIRS with a 0.2K change from nadir to edge of scan.

The biases for the 13.4μm channels on each instrument at the edge of their scans are at least 0.1K different from the nadir view biases (not shown). SEVIRI, with a different scan geometry, has a stronger dependence with an increasing negative bias up to -2.8K with higher zenith angles out to 45° and then the bias reduces for large angles. These large scan angle dependencies in sounding channels suggest that at least part of the apparent bias is due not only to radiometric calibration errors, but also to errors in their assumed spectral response functions, which can modify the channels' weighting functions, and hence their variation with scan angle.

The scan angle dependence of the AMSU-A temperature sounding channels is also significant as illustrated in the lower panels of Figure 11 for Metop-A and NOAA-19 AMSU-A channel 10. This has also been reported by [9]. This bias was found to be consistent between instruments and is stable with time allowing a fixed bias correction to be effective for assimilation. It is surprising that the bias is not more symmetric about nadir for this channel but the radiometer 'sees' parts of the instrument and spacecraft in its side lobes which can cause this asymmetry. Other AMSU-A channels show a similar behaviour although surface sensing channels are more symmetric.

F. Day-Night Differences

The change in bias between day-time and night-time has also been investigated. For SEVIRI the full diurnal cycle can be sampled but for the polar orbiters only one daytime and night-time measurement is taken at one location and so the day minus night difference will strongly depend on the local overpass times. For the platforms included here NOAA-19 and Aqua have early afternoon overpasses and so would be expected to have the biggest diurnal changes. This is clearly illustrated in Table 9 where the day-night bias differences over the ocean in the SEVIRI coverage area are given. The SEVIRI data are averaged over all the daylight hours whereas the polar data are just representative of their overpass times.

As expected the Metop-A and NOAA-17 instruments show smaller diurnal changes. The reason for the diurnal changes is probably originating in the model which does not represent the diurnal thermocline in the sea surface skin temperature and this potentially can introduce localised biases of several kelvin. A map of the day-night differences for SEVIRI and NOAA-19 HIRS (not shown) are similar for both instruments suggesting the differences do originate from the model. The AATSR day-night difference in Table 9 appears to be anomalously high relative to the Metop instruments and it is most likely due to the fact that it has a more effective cloud detection during the day using the visible channel radiances which increase the detection of low uniform cloud making daytime radiances slightly warmer. The other instruments (except SEVIRI) have the same cloud detection during the day and night.

For the 13.4μm temperature sounding channels there is still evidence of a smaller diurnal variation for SEVIRI as shown in Table 9 and perhaps HIRS on NOAA-19, but IASI and AIRS show no significant day-night difference. The 6.5μm water vapour channels on SEVIRI and all the polar sensors show no significant evidence of a day-night difference as they are insensitive to the surface.

VI. SUMMARY AND DISCUSSION

This study has for the first time compiled a comprehensive dataset of the measured radiances from several different satellite instruments and compared them with the

corresponding radiances simulated from a state-of-art NWP 6 hour forecast field. The radiance biases computed are binned according to various different criteria to allow an analysis of the behaviour of these biases for several different parameters (e.g. time, location, scene temperature, incidence angle, etc). The main conclusions from this analysis of the data are summarised here.

Changes in the NWP system can introduce changes in the bias as observed in November 2009 when the model upper tropospheric humidity characteristics were changed which affected the water vapour channels. However by using the double difference technique between different satellite sensors the impact of the model changes can be largely removed.

The trend in the drift of the radiance of the SEVIRI 13.4µm channel using SNOs with other sensors [32] is confirmed using NWP O-B bias statistics presented here. This is caused by the build up of ice on the detector for this channel. The change in bias is not linear with time but has sudden increases periodically. By autumn 2011 the relative bias had reached -2.9K which is averaged over all clear scene temperatures. The GSICS bias monitoring of this channel with respect to IASI suggest a bias of -1.8 K but this is for a normalised 'standard scene temperature' and so cannot easily be compared to the biases presented here. All other SEVIRI channels appear to be stable over the period of this analysis (2009/11) except for the ozone channel which could not be simulated by the NWP model accurately enough to provide a reliable estimate of the bias.

Comparisons between SEVIRI and HIRS channels were more consistent than between SEVIRI and IASI or AIRS because the spectral coverage of HIRS and SEVIRI are more similar, which leads to a similar depth of atmospheric layer being sampled. For strict comparisons this shows the need to integrate the IASI or AIRS radiances over the SEVIRI channel spectral responses. The O-B bias of the 13.4µm channels on SEVIRI, IASI and HIRS (on Metop-A) are all significantly different from each other, highlighting the differences between instruments and the need for bias correction. The O-B bias for the SEVIRI 13.4µm channel on Meteosat-9 is 1.2K larger than for the same channel on Meteosat-8. This inconsistency between the same instruments on different platforms is a concern for climate monitoring purposes and highlights the need for their inter-calibration. In contrast for the 6.2µm water vapour channel the biases are all of similar magnitude, which in this case is due to the biases in the NWP model water vapour distribution dominating.

The behaviour of all 3 HIRS sensors on Metop-A, NOAA-17 and NOAA-19 are similar but the NOAA-17 HIRS channel 1 has an increasing standard deviation in the O-B values between 2009 and 2011 suggesting a degradation in the instrument over time.

The variation of the bias with several different parameters was also investigated. In general the O-B bias becomes more positive with increasing scene temperature for all instruments except AATSR where the bias was found to be independent of scene temperature. This is interesting because the AATSR is the only sensor which has two black bodies one at 260 K and one at 280 K. The other sensors all use space as the cold target and so this result should be investigated further to see if it could have implications for the design of future radiometers for climate monitoring. The change in bias from one edge of the swath to the other (i.e. a function of scan angle) is not insignificant from a climate perspective at about 0.1K for AATSR and IASI, 0.2K for AIRS, and 0.5K for HIRS. For SEVIRI there appears to be a gradual increase in the negative bias away from nadir for the 10.8µm window channel but a minimum in the bias at 45° for the 13.4µm and other sounding channels. For the AMSU microwave radiances there is a strong scan angle dependence which is not symmetrical about nadir but is the same for NOAA-19 and Metop-A and stable in time. The stability of the AMSU microwave radiances with time has been demonstrated although the same channels on different satellites can have quite different biases.

A day-night difference in the O-B bias is observed for clear sky surface sensing channels, probably due to the diurnal thermocline over the ocean not being represented in the model, and also differences in the cloud detection. It is not evident for the upper tropospheric channels.

These results have shown that O-B biases from the Met Office global NWP system can be used as a powerful tool to monitor radiances from all instruments and to intercompare them. This dataset of several years will start to inform the utility of these measurements for climate trend monitoring and exploitation in reanalyses (e.g. ERA-CLIM). It is planned to continue this work within the EUMETSAT NWP SAF activities and obtain longer time series to understand better the bias characteristics of each instrument for generation of climate datasets. Other instruments (e.g. ATMS, CrIS on NPP) may also be included in the data collection and analysis in the future. Finally it would be interesting to compare the biases reported here with the Met Office model with those seen at other NWP centres to help separate out the model biases from the instrument biases.

ACKNOWLEDGMENT

The satellite data were provided by EUMETSAT, ESA and NOAA as part of the real time delivery of data to the Met Office for its operations.

REFERENCES

[1] Newman, S. M., R.O. Knuteson, D.K. Zhou, A.M. Larar, W.L. Smith and J.P. Taylor. Radiative transfer validation study from the European Aqua Thermodynamic Experiment. *Quart. J. Royal Meteorol. Soc.,* vol 135: pp. 277–290. doi: 10.1002/qj.382, 2009.

[2] Harris, B. and G. Kelly. A satellite radiance bias correction for data assimilation. *Quart .J. Royal. Meteorol. Soc.* vol 127 pp. 1453-1468, 2001.

[3] Dee, D. P. and S. Uppala. Variational bias correction of satellite radiance data in the ERA-Interim reanalysis. *Quart. J. Royal Meteorol. Soc.,* vol 135 pp. 1830–1841. doi: 10.1002/qj.493, 2009.

[4] Goldberg M., G. Ohring, J. Butler, C. Cao, R. Datla, D. Doelling, V. Gaertner, T. Hewison, B. Iacovazzi, D. Kim, T. Kurino, J. Lafeuille, P. Minnis, D. Renaut, J. Schmetz, D. Tobin, L. Wang, F. Weng, X. Wu, F. Yu, P. Zhang and T. Zhu. The Global Space-based Inter-Calibration System (GSICS). *Bulletin Am. Meteorol. Soc.*, vol. 92, pp. 467–475 doi:10.1175/2010BAMS2967.1, 2011.

[5] Cao, C., M. Weinreb, and H. Xu. Predicting simultaneous nadir overpasses among polar-orbiting meterological satellites for the intersatellite calibration of radiometers, *J. Atmos. Oceanic Technol.,* vol. 21, pp. 537–542, 2004.

[6] Cao, C., H. Xu, J. Sullivan, L. McMillin, P. Ciren and Y. Hou. Inter-satellite radiance biases for the High Resolution Infrared Radiation Sounders (HIRS) onboard NOAA-15, -16, and -17 from simultaneous nadir observations, *J. Atmos. Oceanic Tech nol.,*vol. 22 (4), pp. 381–395, 2005.

[7] Gopalan, K., W. Linwood Jones, S. Biswas, S. Bilanow, T. Wilheit and T. Kasparis, A time varying radiometric bias correction for the TRMM Microwave Imager. *IEEE Trans. Geoscience and Remote Sensing* vol. 47 pp. 3722- 3730, 2009.

[8] John, V., G. Holl, S. A. Buehler, B. Candy, R.W. Saunders, D. E. Parker. Understanding inter-satellite biases of microwave humidity sounders using global SNOs. *J. Geophys. Res.,* vol. 117, D02305, doi:10.1029/2011JD016349, 2012.

[9] Mo, T. Calibration of the NOAA AMSU-A radiometers with natural test sites. *IEEE Trans. Geoscience and Remote Sensing* vol. 49 pp. 3334-3342, 2011.

[10] Connor, T. C., M. W. Shephard, V. H. Payne, K. E. Cady-Pereira, S. S. Kulawik, M. Luo, G. Osterman, and M. Lampel. Long-term stability of TES satellite radiance measurements. *Atmos. Meas. Tech.,* vol. 4, pp. 1481-1490, 2011.

[11] Geer, A.J., P. Bauer and N. Bormann Solar biases in microwave imager observations assimilated at ECMWF. *IEEE Trans. Geoscience and Remote Sensing* vol. 48 pp. 2660-2669, 2010.

[12] Ohring, G., B. Wielicki, R. Spencer, B. Emery and R. Datla, Satellite Instrument Calibration for Measuring Global Climate Change, *Bull. Amer. Meteorol. Soc.* vol. 1303 pp. 1303-1313, 2005.

[13] GCOS-107: Global Climate Observing System (GCOS), Systematic Observation Requirements For Satellite-Based Products For Climate, World Meteorological Organization, Document WMO/TD No. 1338, http://www.wmo.int/pages/prog/gcos/Publications/gcos-107.pdf, September 2006, 2006.

[14] Allan, R.P, A. Slingo, S.F. Milton, and M.E. Brooks. Evaluation of the Met Office global forecast model using Geostationary Earth Radiation Budget (GERB) data. *Quart. J. Roy. Meteorol. Soc.* vol. 133 pp. 1993–2010, 2007.

[15] Davies T., M.J.P. Cullen, A.J. Malcolm, M.H. Mawson, A. Staniforth, A.A. White and N. Wood. A new dynamical core for the Met Office's global and regional modelling of the Atmosphere. *Quart. J. Roy. Meteorol. Soc.,* vol. 131, pp. 1759-1782, 2005.

[16] Rawlins, F., S.P. Ballard, K. J. Bovis, A.M. Clayton, D. Li, G.W. Inverarity, A.C. Lorenc, and T.J. Payne. The Met Office global four-dimensional variational data assimilation scheme. *Quart. J. Roy. Meteoro.l Soc.,* vol. 133 pp. 347–362. doi: 10.1002/qj.32, 2007.

[17] Li, D. and K.P. Shine. A 4-dimensional ozone climatology for UGAMP models. *UGAMP Internal Report No. 35,* 1995.

[18] Stark, J. D., C. J. Donlon, M. J. Martin, and M. E. McCulloch. OSTIA: An operational, high resolution, real time, global sea surface temperature analysis system. *Proc. OCEANS'07 Europe, Aberdeen, Scotland, IEEE,* Paper 061214-029, 2007 doi: 10.1109/OCEANSE.2007.4302251

[19] Saunders, R., M. Matricardi and P. Brunel. An Improved Fast Radiative Transfer Model for Assimilation of Satellite Radiance Observations. *Quart..J. Roy. Meteorol. Soc.* vol. 125 pp. 1407-1426, doi: 10.1002/qj.1999.49712555615, 1999.

[20] Sherlock, V. ISEM-6: Infrared Surface Emissivity Model for RTTOV-6. *NWP Tech. Rep.* 287 1999 (available from Met. Office Librarian)

[21] Deblonde, G. and S.J. English Evaluation of the FASTEM-2 fast microwave oceanic surface emissivity model. *Tech. Proc. ITSC-XI Budapest, 20-26 Sept 2000* pp. 67-78*,* 2001.

[22] Cameron, J. The effectiveness of the AIRS bias correction of various air-mass predictor combinations. *NWP Technical report 421* 2003 available at: http://www.metoffice.gov.uk/media/pdf/0/9/FRTR421.pdf

[23] Atkinson, N., J. Cameron, B. Candy and S. J. English. Bias correction of satellite data at the Met Office. *Paper in ECMWF/EUMETSAT NWP-SAF Workshop on Bias estimation and correction in data assimilation, ECMWF, 8-11 Nov 2005.* Available at: http://www.ecmwf.int/publications/library/do/references/list/22022006

[24] Hocking J., P.N. Francis and R.W. Saunders. Cloud Detection in Meteosat Second Generation Imagery at the Met Office. *Meteorol. Appl.* Vol. 18 pp. 307–323. DOI: 10.1002/met.239, 2011.

[25] NWP SAF AAPP documentation: Scientific description. NWPSAF-MF-UD-001, 2006. Available at : http://research.metoffice.gov.uk/research/interproj/nwpsaf/aapp/NWPSAF-MF-UD-001_Science.pdf

[26] English S J, J.R. Eyre and J.A. Smith. A cloud-detection scheme for use with satellite sounding radiances in the context of data assimilation for numerical weather prediction. *Quart. J. Roy. Meteorol. Soc*. vol 125 pp. 2359-2378, 1999.

[27] Pavelin, E.G., S. J. English and J. R. Eyre. The assimilation of cloud-affected infrared satellite radiances for numerical weather prediction. *Quart. J. Roy. Meteorol. Soc*. vol. 134 pp. 737-749, doi: 10.1002/qj.243, 2008.

[28] Závody, A.M., C.T. Mutlow and D.T. Llewellyn-Jones. Cloud Clearing over the Ocean in the Processing of Data from the Along-Track Scanning Radiometer (ATSR). *J. Atmos. Oceanic Technol.,* vol. 17, pp. 595–615, 2000. doi: http://dx.doi.org/10.1175/1520-0426(2000)017<0595:CCOTOI>2.0.CO;2.

[29] O'Carroll, A. G., J. G. Watts, L. A. Horrocks, R. W. Saunders, N. A. Rayner: Validation of the AATSR Meteo Product Sea Surface Temperature. *J. Atmos. Oceanic Technol*., vol. 23, pp. 711–726. doi: http://dx.doi.org/10.1175/JTECH1876.1, 2006.

[30] Merchant, C., D. Llewellyn-Jones, R. Saunders, N. Rayner, E. Kent, C. Old, D. Berry, A. Birks, T. Blackmore, G. Corlett. Deriving a sea surface temperature record suitable for climate change research from the along-track scanning radiometers. *Advances in Space Research* vol. 41 (1), pp. 1–11, 2008.

[31] Liang, X. and A. Ignatov. Monitoring of IR Clear-Sky Radiances over Oceans for SST (MICROS). *J. Atmos. Oceanic Technol*., vol. 28, pp. 1228–1242 doi: 10.1175/JTECH-D-10-05023.1, 2011.

[32] Hewison, T. and J. Mueller. Ice Contamination of Meteosat/SEVIRI Implied By Inter-Calibration Against Metop/IASI. IEEE Trans. Geosci. Remote Sensing accepted for publication – this issue, 2013.

[33] Bell, W., S.J. English, B. Candy, N. Atkinson, F. Hilton, N. Baker, S.D. Swadley, W. F. Campbell, N. Bormann, G. Kelly, and M. Kazumori. The assimilation of SSMIS in Numerical Weather Prediction Models. *IEEE Trans. Geoscience and Remote Sensing* vol. 46 pp. 884-900, 2008.

[34] Elliott, D.A. and H. Aumann. Sensitivity of AIRS and IASI radiometric calibration to scene temperature. *Proc. of* SPIE 8153 doi:10.1117/12.893795, 2011.

[35] Ingleby, B., A. Lorenc, K. Ngan, R. Rawlins and D. Jackson. Improved variational analyses using a nonlinear humidity control variable: Formulation and trials. *NWP Tech Report 558.* 2011. Available at: http://www.metoffice.gov.uk/archive/forecasting-research-technical-report-558

Roger W. Saunders received the Ph.D. degree in 1980 from Imperial College, University of London. Since then he has been working in the field of satellite remote sensing at the U.K. Met. Office where he heads a group working on the applications of satellite imagery data for NWP and forecasting. He was also the AMSU-B instrument scientist from 1992-1995 and head of the satellite section at ECMWF from 1995-1999. Most recently he has been leading a group in the European Space Agency to promote the use of satellite data for climate research applications.

Thomas A. Blackmore received a BSc degree in Meteorology in 2005 from the University of Reading. Since graduating he has worked in the Satellite Applications group at the UK Met Office. His research is aimed at improving satellite image data processing, interpretation and assimilation capabilities at the Met Office for NWP and forecasting.

Peter N. Francis gained a D.Phil. degree from Oxford University in 1991, after which he spent ten years working at the Met Office's Meteorological Research Flight facility at Farnborough, UK, carrying out research into the radiative properties of clouds and aerosols. Since 2001, he has been working in the Met Office's Satellite Applications group, primarily carrying out research into the use of MSG imagery data for quantifying the physical properties of clouds and volcanic ash.

Brett Candy Brett Candy received the B.Sc. degree in physics from Imperial College London, UK, in 1993 and the M.Sc. degree in meteorology from the University of Reading, UK, in 2002. Since 1996 he has been with the Met Office where he has worked on several applications of remote sensing data for operational numerical weather prediction. Currently he is working on a scheme to assimilate satellite observations of soil moisture and surface temperature in order to improve the land surface representation within weather forecasting models.

Tim J. Hewison (M'96) received the Ph.D. doctorate in meteorology from the University of Reading, Reading, UK in 2006, based on his thesis on the use of ground-based microwave radiometers for atmospheric temperature and humidity profiling. He is currently a Meteorological Scientist at EUMETSAT, Darmstadt, Germany, concentrating on the calibration of current, past and future satellite instruments. He also currently chairs the Research Working Group of the Global Space-based Inter-Calibration System (GSICS).

TABLE 1.
CHANNELS FOR WHICH O-B STATS WERE COMPUTED. THE COLUMN ON THE RIGHT IS THE CHANGE IN BRIGHTNESS TEMPERATURE FOR A +10% CHANGE IN TOTAL COLUMN OZONE FOR THE IASI CHANNEL.

IASI Channel	IASI cm^{-1}	AIRS Channel	AIRS cm^{-1}	HIRS Channel	SEVIRI Channel	AATSR Channel	Ozone Sensitivity
92	667.75	75	667.78	1			0.00
141	680	123	680.14	2			0.02
179	689.5	138	689.49	3			0.02
212	697.75	168	697.71				0.00
242	705.25	193	704.72	4			0.00
246	706.25	198	706.14				0.03
280	714.75	227	714.48	5			0.06
345	731	295	734.15				0.04
381	740	318	741.29				0.06
434	753.25	355	753.06	7	11		0.06
457	759	375	759.57				0.05
546	781.25	475	801.10				0.03
756	833.75	528	820.83		10	1	0.00
1121	925	787	917.31	8		2	0.00
1133	928	791	918.75		9		0.00
1579	1039.5	1088	1039.23	9	8		2.40
1991	1142.5	1260	1135.57				0.04
2019	1149.5				7		0.05
2245	1206	1263	1216.97				0.00
2741	1330	1449	1330.98	11	6		0.00
3029	1402	1583	1402.15				0.00
3339	1479.5	1681	1476.25		5		0.00
3522	1525.25	1756	1524.35	12	5		0.00
3540	1529.75			12	5		0.00
3653	1558	1794	1563.71		5		0.00
3943	1630.5				5		0.00
5130	1927.25						0.00
		1873	2188.76	13			0.00
		1897	2210.85	14			0.00
6350	2232.25	1924	2236.23	15			0.00
		1937	2248.65	16			0.00
6463	2260.5	1948	2259.26				0.00
6601	2295	1988	2298.71				0.00
6962	2385.25	2106	2385.23				0.00
6980	2389.75	2111	2390.11				0.00
6997	2394	2115	2394.03	17	4		0.00
7424	2500.75	2189	2492.08	18	4		0.00
8007	2646.5	2363	2648.75		4		0.00
		2377	2664.14	19	4	3	0.00

TABLE 2
TIME LINE OF CHANGES IN MET OFFICE FORECAST MODEL

Date	Model change
20 Aug 2009	Start assimilation of NOAA-19 HIRS and AMSU radiances.
10 Nov 2009	Change of model levels from 50 to 70 and model top raised from 0.1hPa to 0.01hPa.
10 Nov 2009	Change in bias correction of radiosonde relative humidity.
17 Dec 2009 to 9 Feb 2010	NOAA-17 HIRS not assimilated.
9 Mar 2010	DMSP F-16 SSMIS window channels assimilated operationally – clear scenes only over ocean.
2 Nov 2010	Modify AIRS channel selection and assumed observation errors.
2 Nov 2010	SSMIS channels 21,22 introduced to improve mesospheric/upper stratospheric analysis .
2 Nov 2010	Introduce Meteosat-9 clear sky window and water vapour channel radiances.
20 July 2011	Introduce GOES-E+W clear sky window and water vapour channel radiances.
20 July 2011	Use more IASI channels over land.
20 July 2011	Change in humidity control variable from relative humidity to normalised pseudo relative humidity [35].

TABLE 3
INSTRUMENTS AND CHANNELS FOR WHICH BIAS MONITORING STATISTICS WERE COLLECTED DURING 2009-2011.

Geostationary Satellite	Instrument	Channels	Source	Comments
Meteosat-8	SEVIRI	8 IR	EUMETCAST	Only when Met-9 is unavailable
Meteosat-9	SEVIRI	8 IR	EUMETCAST	
Polar-orbit Satellite	**Instrument**	**Channels**	**Source**	**Comments**
Metop-A	IASI	See Table 1	EUMETCAST	
	HIRS	9 IR	EUMETCAST	
	AMSU-A	5 MW	EUMETCAST	From Aug-10
	MHS	5 MW	EUMETCAST	From Aug-10
Aqua	AIRS	See Table 1	NESDIS	Occasional outages
NOAA-17	HIRS	9 IR	NESDIS	Gap after mid Dec-09
NOAA-19	HIRS	9 IR	NESDIS	
	AMSU-A	5 MW	NESDIS	From Aug-10
	MHS	5 MW	NESDIS	From Aug-10
ENVISAT	AATSR	3 IR Nadir 3 IR Fwd	FTP ESRIN	From 1 Sep-10. No data after 8 April 2012.

TABLE 4
SAMPLING OF RADIANCES FOR BIAS ANALYSIS

Parameter	SEVIRI	HIRS	IASI	AIRS	ATSR	AMSU/MHS
Time	Hrly	12 hrs	12 hrs	12 hrs	12 hrs	12 hrs
Spatial	1 in 4	All	1 in 4	1 in 9	10 arc min	All
Lat	30^o bands	30^o bands	30^o bands	30^o bands	30^o bands	30^o bands
Long	30^o bands	30^o bands	30^o bands	30^o bands	30^o bands	30^o bands
Chans	8 IR	19 IR	Table 1	Table 1	Table 1	15/5 MW
Incidence angles	10^o bins	10^o bins	10^o bins	10^o bins	10^o bins	10^o bins
Surface type	sea/ land/ ice	sea/ land/ ice	sea/ land/ ice	sea/ land/ ice	sea	sea/ land/ ice
Cloud	Clear cloud Day/ night	Clear cloud Day/ night	Clear/cloud Day/ night	Clear/cloud Day/ night	Clear/ cloud Day/ night	Clear/ MW cloudy/ Rain
Scene radiance	10 bins	10 bins	10 bins	10 bins	10 bins	10 bins

TABLE 5.
NUMBER OF OBSERVATIONS IN MILLIONS COLLECTED FROM 19 NOV 2008 TO 27 NOVEMBER 2011 (AATSR PERIOD FROM 1 SEP 10; MICROWAVE INSTRUMENTS FROM 18 AUG 2010).

Geostationary Satellite	Instrument	Total no. Radiances $X10^6$	No. of clear radiances $X10^6$
Meteosat-9	SEVIRI	8763	2756
Polar-orbit Satellite	**Instrument**		
Metop-A	IASI	235.9	42.2
	HIRS	569.2	162.9
	AMSU/MHS	275.5	179.3
Aqua	AIRS	163.1	26.0
NOAA-17	HIRS	488.2	144.2
NOAA-19	HIRS	453.3	124.7
	AMSU/MHS	309.7	246.6
ENVISAT	AATSR	N/A	41.2

TABLE 6.
THE MEAN GLOBAL O-B CLEAR SKY BIASES OVER SEA FOR EACH OF THE HIRS INSTRUMENTS DURING 2010. CHANNELS 13-19 ARE FOR NIGHT-TIME ONLY.

	NOAA-17			NOAA-19			Metop-A		
HIRS	**Sea**	**Sea**	**No. Obs**	**Sea**	**Sea**	**No. Obs**	**Sea**	**Sea**	**No. Obs**
Chan	**O-B (K)**	**St Dev (K)**	**X10^6**	**O-B (K)**	**St Dev (K)**	**X10^6**	**O-B (K)**	**St Dev (K)**	**X10^6**
1	-1.08	4.40	24.5	0.65	1.68	31.1	-0.60	1.16	31.4
2	-1.47	0.70	24.5	-0.72	0.58	31.1	-0.62	0.35	31.4
3	-0.85	0.49	24.5	-0.54	0.29	31.1	-0.59	0.25	31.4
4	-0.16	0.24	24.5	-0.46	0.24	31.1	-0.52	0.25	31.4
5	-0.33	0.27	24.5	-0.80	0.30	31.1	-0.32	0.28	31.4
7	-0.60	0.52	24.5	-0.91	0.55	31.1	-0.78	0.54	31.4
8	-0.80	0.84	24.5	-0.82	0.94	31.1	-0.78	0.91	31.4
9	2.23	2.52	24.5	2.63	2.74	31.1	2.60	2.75	31.4
11	0.94	1.15	24.5	0.70	1.11	31.1	0.81	1.16	31.4
12	0.13	1.65	24.5	-0.09	1.65	31.1	-0.18	1.65	31.4
13	-1.35	0.55	11.9	0.24	0.58	13.7	-0.18	0.52	14.9
14	-0.90	0.36	11.9	-0.92	0.36	13.7	-0.90	0.37	14.9
15	-1.05	0.32	11.9	-0.72	0.33	13.7	-1.11	0.37	14.9
16	0.90	0.26	11.9	-1.28	0.39	13.7	-1.50	0.48	14.9
17	-1.37	0.67	11.9	-1.31	0.72	13.7	-0.94	0.70	14.9
18	-0.67	0.90	11.9	-0.90	1.00	13.7	-0.70	0.99	14.9
19	-0.65	0.89	11.9	-0.84	0.99	13.7	-0.65	0.98	14.9

TABLE 7.
METEOSAT-9 GLOBAL O-B CLEAR SKY BIASES OVER SEA DURING 2010 FOR EACH OF THE SEVIRI INFRARED CHANNELS. CHANNEL 4 IS FOR NIGHT-TIME ONLY.

SEVIRI Channel	O-B (K)	O-B St. Dev (K)	Obs X10^6
4	-2.02	0.76	232.4
5	-0.02	1.45	453.9
6	0.87	1.07	453.9
7	-0.48	0.70	453.9
8	3.39	2.70	453.9
9	-0.38	0.76	453.9
10	-0.49	0.82	453.9
11	-2.16	0.68	453.9

TABLE 8.
MEAN GLOBAL O-B CLEAR SKY BIASES OVER THE SEA FOR THE AATSR NADIR AND FORWARD VIEW RADIANCES FOR THE PERIOD 1 SEP 2010 TO 31 AUG 2011.

AATSR Chan	Viewing angle	Wavelength (μm)	No. Obs X10^6	O-B (K)	St Dev (K)	Day/ Night
1	nadir	12.0	33.2	-0.479	0.649	d/n
2	nadir	11.0	33.2	-0.202	0.577	d/n
3	nadir	3.7	17.3	-0.164	0.409	n
4	forward	12.0	33.2	-0.595	0.804	d/n
5	forward	11.0	33.2	-0.266	0.710	d/n
6	forward	3.7	17.3	-0.291	0.443	n

TABLE 9.
DAY-NIGHT RADIANCE DIFFERENCES IN K FOR IR WINDOW (~10.8 MICRON), CO_2 (~13.4 MICRON) AND UPPER TROPOSPHERIC HUMIDITY (~6.5 MICRON) CHANNELS. THE DATA ARE OVER CLEAR SKY OCEAN FOR THE PERIOD 1 SEP 2010 TO 31 AUG 2011, AND ARE RESTRICTED TO THE REGION 60^{O}N – 60^{O}S, 60^{O}W – 60^{O}E.

Instrument and (channel number)	Overpass time (UTC)	10.8 micron channel	13.4 micron channel	6.5 micron channel
SEVIRI (9, 11, 5)	Hourly	0.30 K	0.14 K	0.03 K
HIRS NOAA-19 (8,7,12)	14:00	0.25 K	0.08 K	-0.02 K
HIRS NOAA-17 (8,7,12)	11:00	0.03K	0.03K	0.09 K
HIRS Metop (8,7,12)	10:00	0.08 K	0.04 K	0.11 K
IASI (1133, 434, 3522)	10:00	0.04 K	0.05 K	0.02 K
AIRS (787, 355, 1756)	13:30	0.12 K	0.04 K	-0.03 K
AATSR (2)	10:15	0.14 K	N/A	N/A

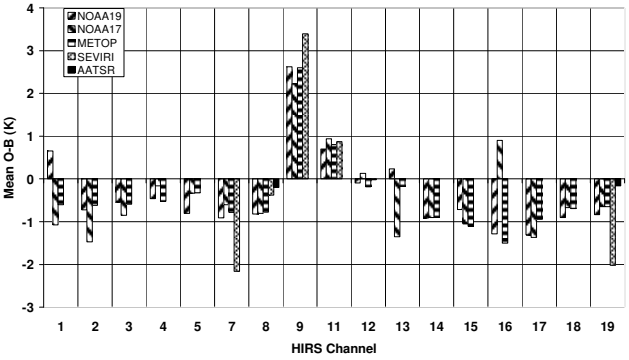

Figure 1. Global mean O-B biases of HIRS channels over the sea for 2010. The shortwave channels are only for night-time data. The corresponding SEVIRI and AATSR channel biases are also plotted for those channels which are common in wavelength.

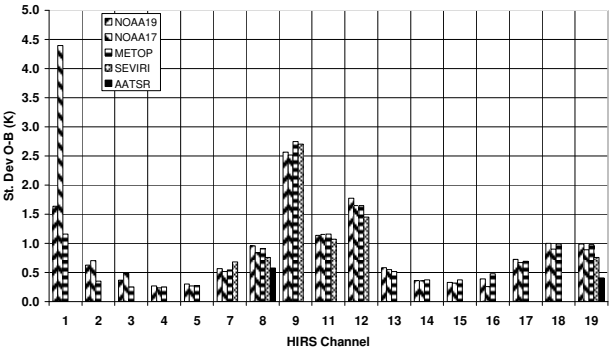

Figure 2. As for Figure 1 but the global mean standard deviation of the O-B difference for HIRS and common SEVIRI and AATSR channels.

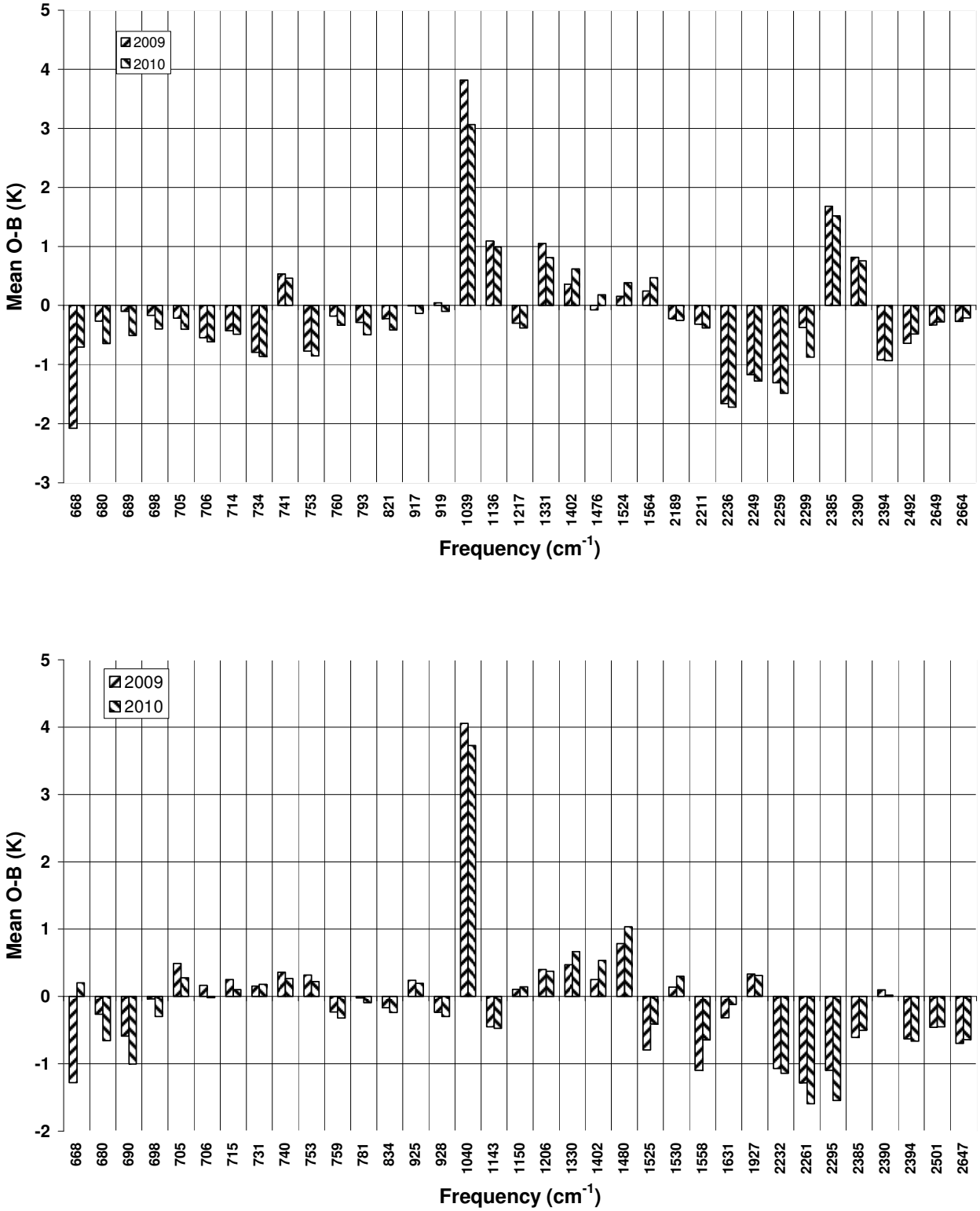

Figure 3. AIRS (top panel) and IASI (bottom panel) mean O-B statistics for 2009 and 2010.
The shortwave channels are for night-time only.

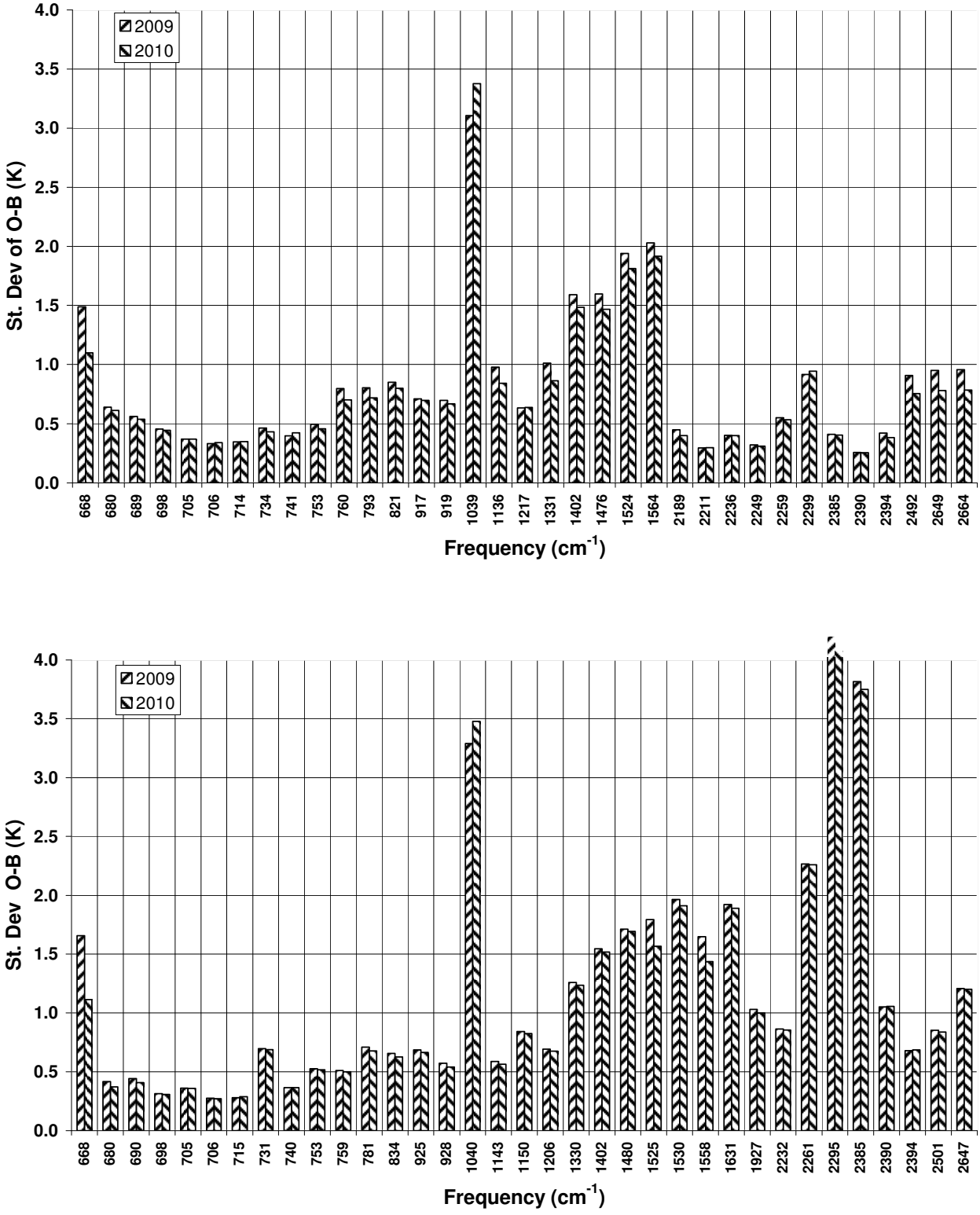

Figure 4. AIRS (top panel) and IASI (bottom panel) standard deviation of O-B for 2009 and 2010. The shortwave channels are for night-time only.

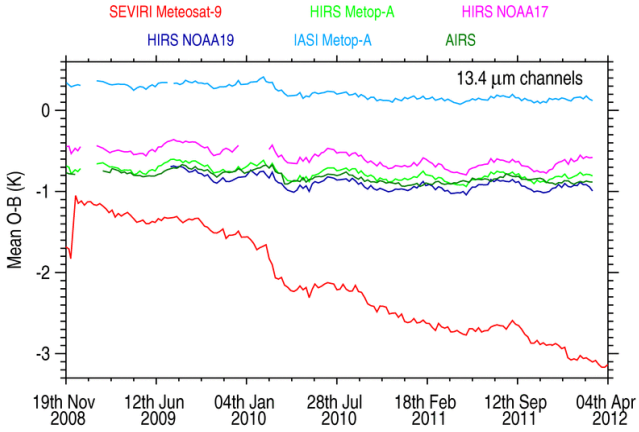

Figure 5. Plots of the O-B mean bias for the 13µm channels from SEVIRI (channel 11), NOAA-17, NOAA-19 and Metop-A HIRS (channel 7) AIRS (channel 355) and IASI (channel 434). All plots are just over the SEVIRI area (i.e. 60N-60S, 60W-60E) for clear sky ocean points.

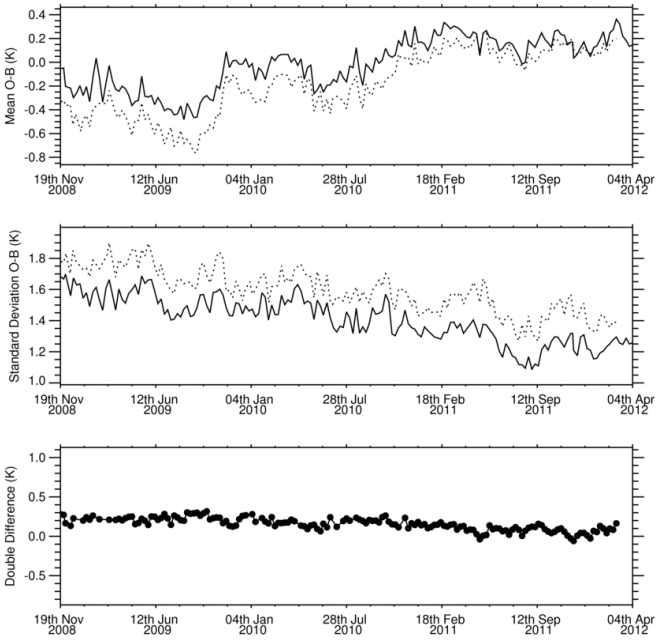

Figure 6. Plots of 6.2/6.7µm channels from SEVIRI (channel 5) as solid line and Metop-A HIRS (channel 12) as dotted line. Upper panel shows the O-B global mean bias, middle panel the standard deviation of the difference and lower panel the double difference. All plots are just over the SEVIRI area for clear sky ocean points.

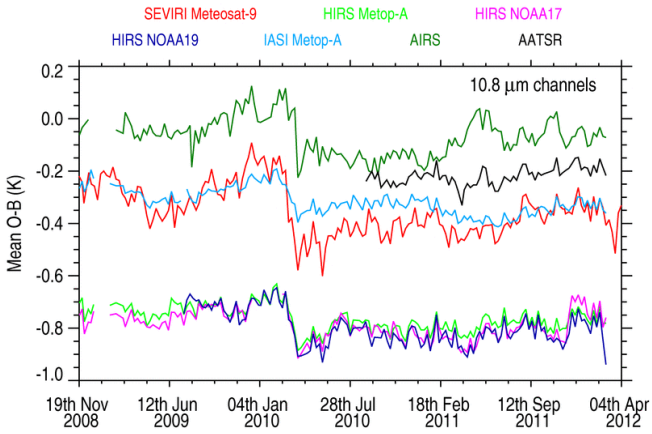

Figure 7. Plots of the O-B mean bias for the 11µm window channels from SEVIRI (channel 9), NOAA-17, NOAA-19 and Metop-A HIRS (channel 8), AATSR (channel 2), AIRS (channel 787) and IASI (channel 1133). All plots are just over the SEVIRI area (i.e. 60N-60S, 60W-60E) for clear sky ocean points.

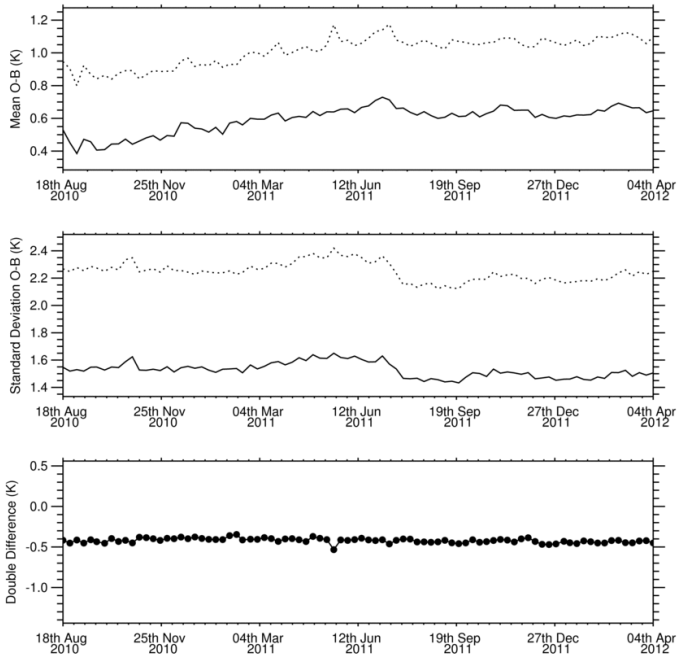

Figure 8. Plots of MHS upper tropospheric water vapour channel (3) from NOAA-19 (dotted) and Metop-A (solid). Upper panel shows the O-B global mean bias, middle panel the standard deviation of the difference and lower panel the double difference. All plots are for global coverage.

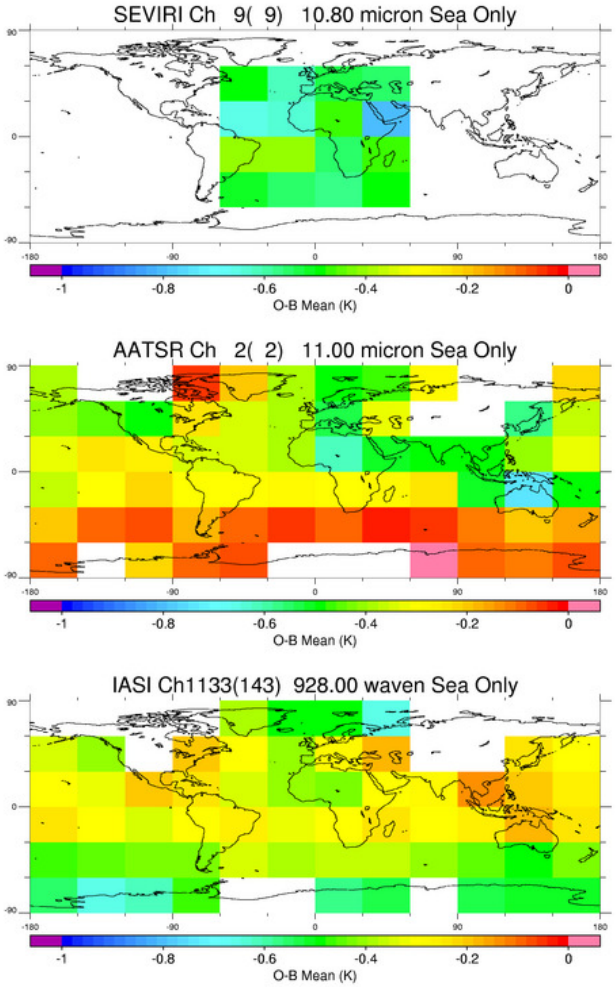

Figure 9. Map of SEVIRI, AATSR and IASI clear sky window channel (11μm) O-B statistics for sea points only for 2010 except AATSR which is for Sept 2010 to March 2011.

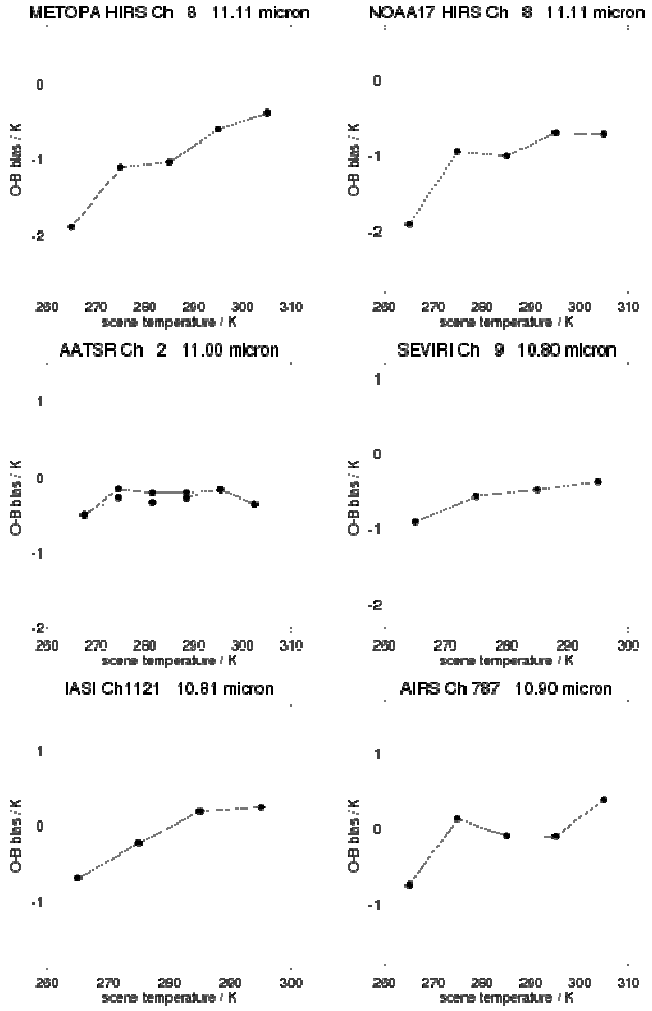

Figure 10. The changes in O-B bias for scene temperature for the 11μm window channels on HIRS on Metop-A and NOAA-17 (top panels), AATSR and SEVIRI (middle panels) and IASI and AIRS (lower panels). These are global clear sky statistics over the ocean for 2010 except AATSR which is from Sept 2010 to Aug 2011. The dashed line on the AATSR plot is for the forward view.

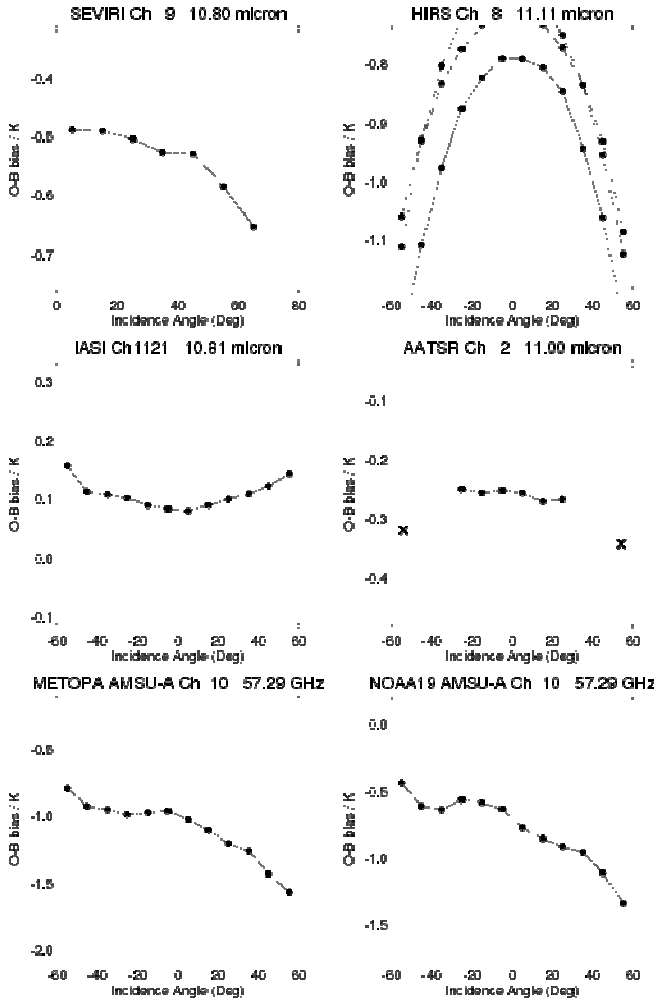

Figure 11. Plots of the mean clear sky bias for the 11µm channels of SEVIRI, HIRS, IASI, AATSR and ASMU-A as a function of incidence angle at the surface. The 3 lines on the HIRS plot correspond to data from Metop-A, and NOAA-17/19. The crosses on the AATSR plot correspond to the forward view. The data are over the ocean for 2010 except AATSR which is from Sept 2010 to Aug 2011.